Letter

Enlarged deformation region in neutron-rich Zr isotopes promoted by the second intruder orbit

W. Horiuchi [1,2,3,4,*] T. Inakura [5] S. Michimasa [6] and M. Tanaka [3]

[1]*Department of Physics, Osaka Metropolitan University, Osaka 558-8585, Japan*

[2]*Nambu Yoichiro Institute of Theoretical and Experimental Physics (NITEP), Osaka Metropolitan University, Osaka 558-8585, Japan*

[3]*RIKEN Nishina Center, Wako 351-0198, Japan*

[4]*Department of Physics, Hokkaido University, Sapporo 060-0810, Japan*

[5]*Laboratory for Zero-Carbon Energy, Institute of Innovative Research, Tokyo Institute of Technology, Tokyo 152-8550, Japan*

[6]*Center for Nuclear Study, The University of Tokyo, 2-1 Hirosawa, Wako, Saitama 351-0198, Japan*

(Received 21 February 2023; accepted 12 April 2023; published 28 April 2023)

Nuclear deformations and density profiles of neutron-rich even-even Zr isotopes are investigated by using the Skyrme-Hartree-Fock-Bogoliubov method. Large quadrupole and hexadecapole deformations are predicted along with large enhancement of the total reaction cross sections at the neutron number $N = 60$–74. Strong nuclear deformation starting at $N = 60$ is induced by the occupation of the intruder orbit with the asymptotic quantum number $[nn_z\Lambda]\Omega = [550]1/2$ originating from the spherical $0h_{11/2}$ orbit. The deformation region is further enlarged from $N = 72$ to 74 owing to the occupation of the next intruder orbit with $[530]1/2$ originating from the spherical $1f_{7/2}$ orbit. This characteristic nuclear deformation is crucially reflected in a systematic behavior of the nuclear radii and the density profiles near the nuclear surface.

DOI: 10.1103/PhysRevC.107.L041304

Nuclear deformation gives a significant impact on the change of the nuclear density profiles near the nuclear surface, resulting in the enhancement of the nuclear radii [1–11]. In the nuclear chart, there exist some regions where a nuclear system exhibits unexpectedly large deformation. The most striking examples are the island-of-inversion nuclei around the neutron numbers $N = 20$ [12] and 40 [13], where the ordering of the single-particle orbits near the Fermi level is inverted by the intruder orbit coming from a higher shell in the spherical limit. The intruder orbit is highly elongated along the quantization axis in the intrinsic frame and thus its occupation induces a deformed nuclear shape, i.e., diffused nuclear surface in the laboratory frame. Theoretical analyses [9,11] showed that the shell evolution in the island-of-inversion regions results in diffusing the density profile near the nuclear surface and increases the nuclear radii. Here, we study the development of nuclear deformation in $_{40}$Zr isotopes, where the intruder configuration is expected to play a crucial role throughout the isotope chain.

Zr isotopes exhibit complicated isotope dependence on nuclear deformation. Experiments confirmed isotopes between ^{78}Zr [14] and ^{114}Zr [15] and theories predicted that Zr isotope persists to at least ^{128}Zr [16]. The neutron-deficient $N = Z$ nucleus ^{80}Zr was predicted having largely deformed ground state [17,18]. The stable nuclei $^{90–96}$Zr and ^{98}Zr are spherical, and ^{100}Zr becomes again largely deformed ground state. The large quadrupole deformation in $^{100–106}$Zr was confirmed experimentally by measurements of the electric-quadrupole ($E2$) transition strengths in even-N isotopes [19,20] and the $E2$ moments for odd-N isotopes [21]. Furthermore, the measurements of the first 2^+ excitation energies in ^{108,110}Zr strongly indicate that the large deformation persists up to ^{110}Zr [22,23]. The quadrupole deformations along the Zr isotope chain were theoretically evaluated by mean-field [24–27] and shell model [28,29] approaches. Some Zr isotopes are candidates of tetrahedral nuclei [30,31] and/or shape coexistence phenomena [32–36].

To extract the quadrupole deformation of unstable nuclei, the reduced $E2$ transition strength $B(E2)$ from the first 2^+ state is one of the standard physical quantities for even-even nuclei. The $B(E2)$ value is experimentally deduced by measuring angular distributions of the cross sections of the Coulomb excitation or the lifetime of the first 2^+ state. Hadronic probes through nuclear interactions can also be used. The proton inelastic scattering at intermediate energy is theoretically established as a probe of the quadrupole deformation [37], and this method was successfully adopted for many experiments for exotic radioactive nuclei [38–42].

Here, we focus on the observation of the total reaction cross section (σ_R) as a measure of quadrupole deformation. The σ_R or interaction cross section measurement has often been performed to extract the size of nuclei, especially in nuclei far from the β stability line because the cross section is extremely large by $\approx$1 barn. Furthermore, the theoretical framework linking the cross section to the nuclear matter radius is well tested and established [5,8,43–53]. Therefore, σ_R is a promising observable for detecting anomalies of the nuclear structure appearing along isotopic chains [2,6,54–72]. It should be noted that in the island-of-inversion nuclei, Ne and Mg isotopes, the strong quadrupole deformation starting at around $N = 20$ was successfully probed as an enhancement of the σ_R

*whoriuchi@omu.ac.jp

value [1–8]. A systematic measurement of the cross sections along the Zr isotopic chain sheds light on the emergence of the quadrupole deformation. We will discuss later its capability as a quantitative probe of the quadrupole deformation of the Zr region.

In this paper, we generate the density distributions of neutron-rich even-even Zr isotopes by the Skyrme-Hartree-Fock-Bogoliubov (HFB) model using the HFB solver, HFBTHO [73]. The SkM* interaction is employed [74] as it is known to reasonably describe nuclear deformations. A standard mixed-type pairing interaction is used [75]. Note that the HFBTHO code assumes an axial symmetry in the nuclear density. To access the effects of this constraint and the pairing interaction, we compute the Skyrme-HF plus Bardeen-Cooper-Schrieffer(BCS)–type pairing (HF+BCS) in three-dimensional coordinate space. The BCS pairing strength is adjusted to reproduce the pairing rotational energy around ^{90}Zr [76]. To see the effect of nuclear deformation, we also perform the spherical-constrained HF calculation with the filling approximation [77].

Once we obtain the intrinsic density distributions, the density distributions in the laboratory frame are obtained by taking an average over angles as prescribed in Ref. [5]. This density distribution is used as a direct input to the calculation of σ_R. Here, we evaluate σ_R on a carbon target as it has the sensitivity of the nuclear density profiles near the nuclear surface [78]. The Glauber theory [79] with the nucleon-target formalism [43] is used to evaluate the optical phase-shift function. The inputs to the theory are the density distributions of the projectile and target nuclei and the profile function. A standard parameter set of the profile function is tabulated in Ref. [80] and has been well tested in high-energy nucleus-nucleus collisions including unstable nuclei [5,8,47–53]. Thus, σ_R properly reflects the information on the density profile of the projectile nucleus.

Figure 1 displays calculated quadrupole deformation parameters β_2 of even-even Zr isotopes with $N = 50$–82 together with experimentally extracted $|\beta_2|$ values [19,20]. A negative β_2 value means oblate deformation. The isotopes with $N = 50$–58 are spherical and show large and sudden enhancement of the β_2 value at $N = 60$. This large deformation $\beta_2 \approx 0.4$ is kept up to $N = 74$. At $N = 76$, the deformation of the ground state is suddenly changed to an oblate shape, $\beta_2 \approx -0.2$, and the isotopes at $N = 78$–82 become spherical again. The emergence of nuclear deformation will be discussed later in detail.

Though there are small quantitative differences, all the theoretical models, HFB, HF+BCS, and HF, show similar isotope dependence and reproduce the trend of the experimental data, especially, the sudden onset of the deformation at $N = 60$. Note that this large prolate deformation is also supported by the large quadrupole deformation $\beta_2 = 0.4283(317)$ deduced from the $E2$ moment measurement for ^{101}Zr ($N = 61$) [81].

We note that the HFB and HF+BCS results are almost identical, indicating that the nuclear deformation and pairing correlations in Zr isotopes are well described in the HF+BCS approach as well. The HF results, which do not include the pairing correlations, mostly follow the HFB and HF+BCS

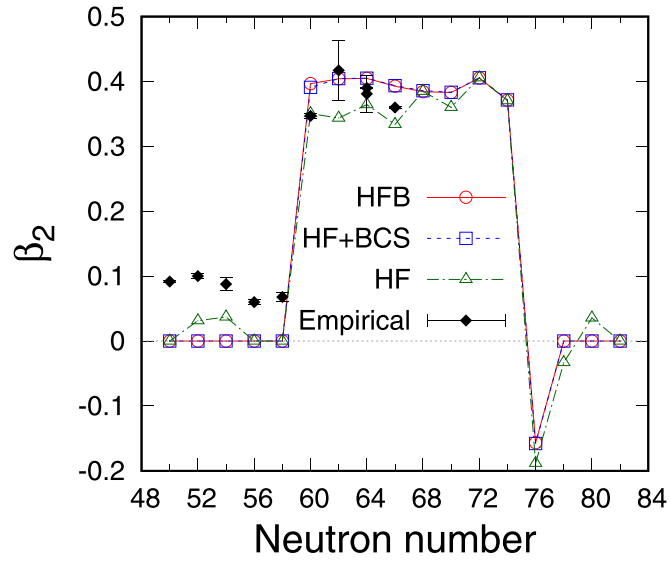

FIG. 1. Quadrupole deformation parameters β_2 of even-even Zr isotopes as a function of neutron number calculated with the HFB, HF+BCS, and HF models. Experimental $|\beta_2|$ values are taken from Refs. [19,20]. The horizontal thin dotted line indicates $\beta_2 = 0$.

ones but some deviations are found. This is because the HF calculations exhibit triaxial deformation: $\gamma = 14^\circ$, 14°, and 20° for these nuclei with $N = 62$, 64, and 66, respectively. We confirm that no triaxial deformation is obtained in the HF+BCS calculations. The resulting ground-state wave function is found to be an axially symmetric, prolate or oblate shape, i.e., the γ value is 0° or 60°. The pairing interaction plays a role in suppressing the triaxiality of Zr isotopes in this mass region.

It is well known that the isotope dependence of nuclear radii follows that of the nuclear quadrupole deformation in light to medium mass nuclei [1,3–11]. Figure 2 plots the root-mean-square (rms) point-proton (r_p) and neutron (r_n) radii of even-even Zr isotopes calculated by the HFB, HF+BCS, HF, and spherical-constrained HF models. The experimental point-proton radii [82] are also plotted for comparison. The results with the HFB and HF+BCS models nicely reproduce the experimental values, while the ones with the spherical-constrained HF calculation do not explain the experimental proton radii at $N = 60$ and 62. The nuclear deformation is essential to account for the proton radii. At a closer look, the HF results show small deviations as their quadrupole deformations are not large enough as shown in Fig. 1 due to the lack of pairing correlations.

The reproducibility in β_2 and r_p clearly shows the validity of the present theoretical models. We note that the point-neutron radii also behave like the proton ones. This coincident trend of the proton and neutron radii suggests that both protons and neutrons associate to develop nuclear deformation.

As mentioned before, these density profiles can be used as the inputs to the Glauber theory, allowing us to relate the rms matter radius (r_m) to a high-energy reaction observable, σ_R. Figure 3 plots σ_R on a carbon target at 300 MeV/nucleon, which is a typical condition of the recent systematic measurements [2,6,54]. The trend of σ_R reflects the behavior of

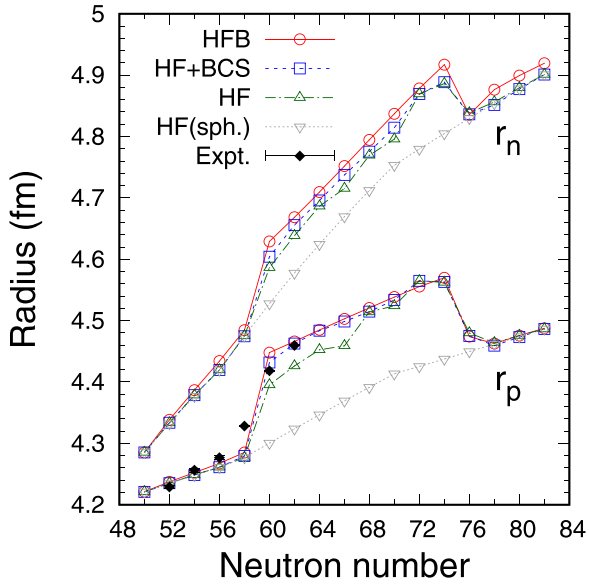

FIG. 2. Rms point-proton (r_p) and neutron (r_n) radii of even-even Zr isotopes as a function of neutron number calculated with the HFB, HF+BCS, HF, and spherical-constrained HF models. The experimental point-proton radii are deduced from Ref. [82].

the matter radii displayed in Fig. 4: a sudden enhancement at $N = 60$ and reduction at $N = 76$ compared to the spherical one, which only shows monotonic increases of the matter radii. In σ_R, this deformation effect, i.e., the difference from the spherical-constrained HF calculation, is approximately 100 mb, which is enormously large recalling that the cross-section increases in Ne and Mg isotopes are typically a few tens of mb, at most ≈50 mb [5]. Since this enhancement corresponding to the relative change of 4% (≈100 mb/2500 mb)

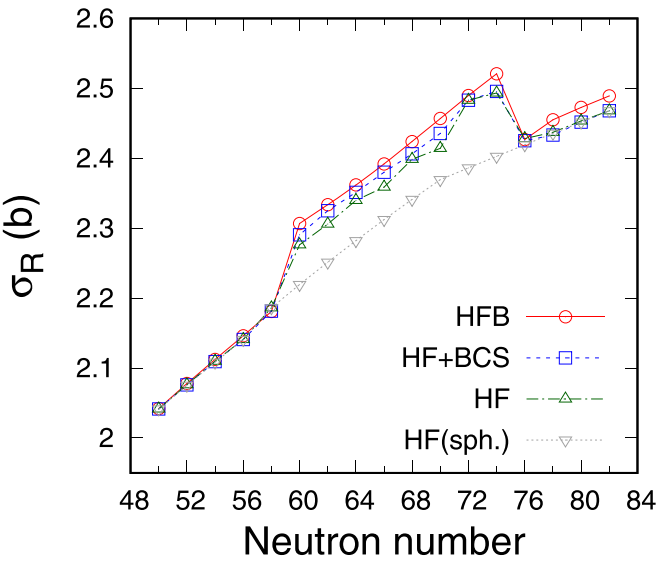

FIG. 3. Total reaction cross sections on a carbon target of even-even Zr isotopes at 300 MeV/nucleon as a function of neutron number calculated with the HFB, HF+BCS, HF, and spherical-constrained HF models.

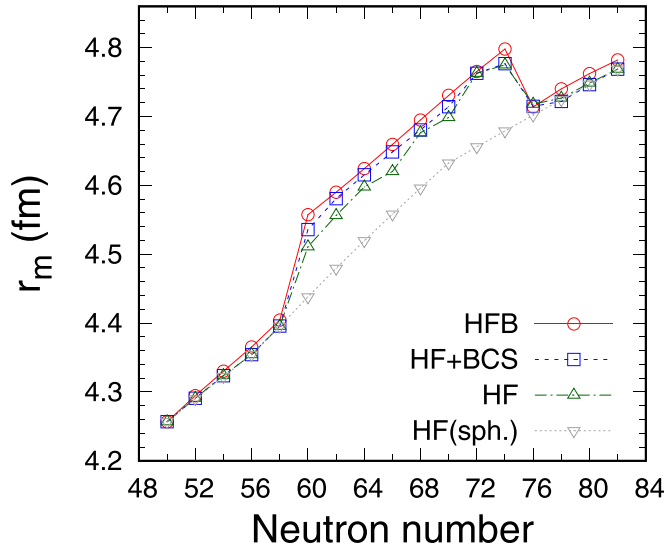

FIG. 4. Same as Fig. 2 but for matter radii (r_m).

is large enough to distinguish experimentally under the typical experimental condition [2,6,54], it is anticipated that the region beyond $N = 70$, which is the subshell closure of sdg orbits, which will be focused on later, can be accessed through the σ_R measurement with sufficient experimental precision using the high-intensity radioactive ion beams of 0.1–1 counts per second in which the recent sophisticated facility can be supplied [83,84]. On the other hand, it seems difficult to reach the $N = 70$ isotope for the moment by using the β-γ delay coincidence technique, that was adopted for the $B(E2)$ measurement of ^{106}Zr [20] because a parent Y isotope production rapidly decreases as the neutron number increases.

The mechanism of the large cross-section enhancement due to large quadrupole deformation can be explained by the occupation of the intruder orbits. In such a largely deformed region, the asymptotic quantum number $[nn_z\Lambda]\Omega$ is useful to classify the single-particle orbits [85]. In $60 \leqslant N \lesssim 70$, the $[550]1/2$ orbit, which comes from the spherical $0h_{11/2}$ orbit, plays a role to induce the large quadrupole deformation. When the spherical sdg orbits are fully occupied at $N \approx 70$, the nuclear system will be a spherical shape if the shell gap between the spherical sdg and $0h_{11/2}$ orbits is sizable. However, the large nuclear deformation is kept up to $N = 74$. Another mechanism is needed for explaining this enlargement of the deformation region. We remark that the enlargement of the deformation region at $N \approx 72$ in Zr isotopes is seen in several previous papers [24,27] but its mechanism was not discussed.

To clarify the reason for the enlarged deformation region at $N = 72$–74, we plot in Fig. 5 the neutron single-particle energies of ^{112}Zr as a function of the quadrupole deformation parameter. The deformation energy, which is measured from that with the spherical shape ($\beta_2 = 0$), is also plotted as a guide. ^{112}Zr has the energy minimum at $\beta_2 = 0.4$. Since the nuclear deformation is so large, the elongated, next intruder orbit with $[530]1/2$ coming from the spherical $1f_{7/2}$ orbit is occupied and further enhances the nuclear radius. This "second" intruder orbit acts to form the shell gaps at $N = 72$ and

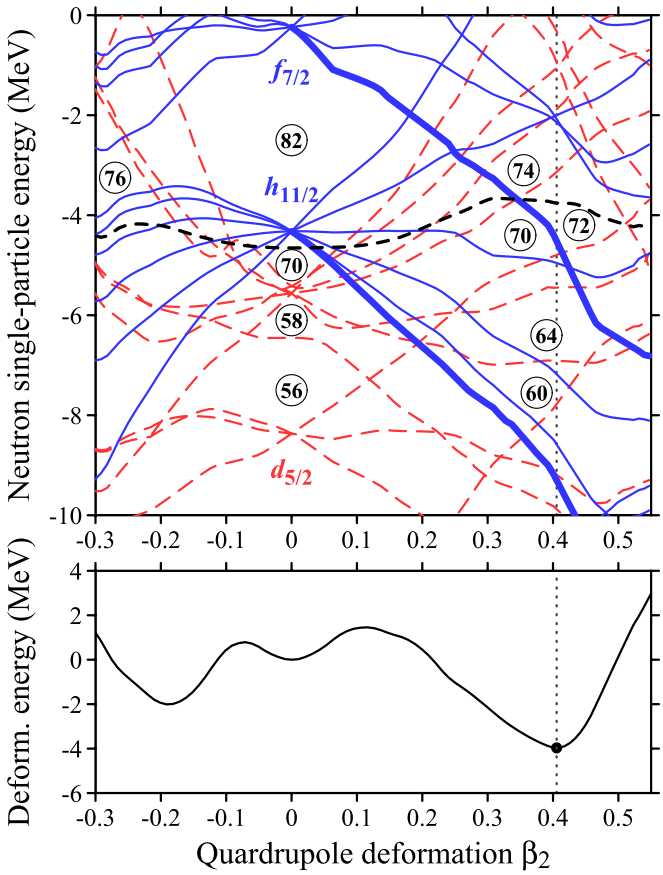

FIG. 5. Neutron single-particle and deformation energies of ^{112}Zr as a function of quadrupole deformation parameter β_2. Thin solid and dashed curves in the upper panel represent negative and positive parity single-particle states, respectively. Thick solid curves indicate the [550]1/2 and [530]1/2 orbits, which comes from the spherical $0h_{11/2}$ and $1f_{7/2}$ orbits at $\beta_2 = 0$, respectively. The thick dashed curve denotes the neutron chemical potential. A vertical thin dotted line indicates the β_2 value at the energy minimum which corresponds to the ground state of ^{112}Zr for a guide to the eye.

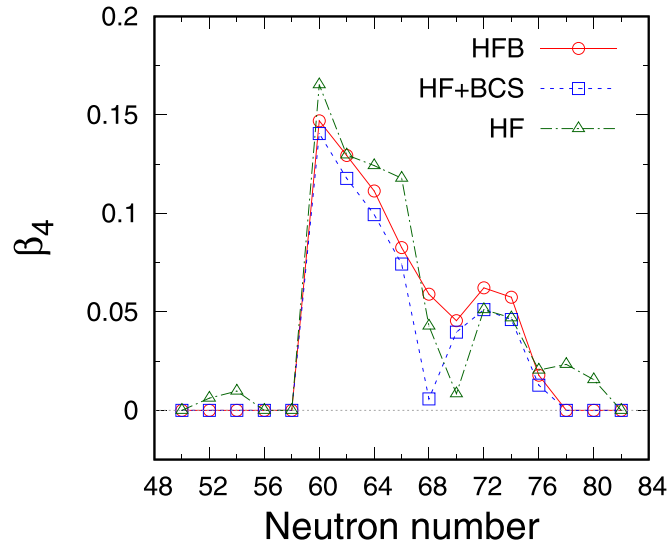

FIG. 6. Hexadecapole deformation parameters β_4 of even-even Zr isotopes as a function of neutron number calculated with the HFB, HF+BCS, and HF models. The horizontal thin dotted line indicates $\beta_4 = 0$.

74, and hence such a large deformation is stabilized. On the other hand, this single-particle energy diagram indicates that the shell gap at $N = 76$ does not appear in prolate deformation but in oblate deformation around $\beta_2 \approx -0.2$. This situation may indicate the sudden change from prolate to oblate deformation at $N = 76$.

We remark that this sort of enlargement of the deformation regions can also be seen in Mg isotopes. In the neutron-rich Mg isotopes, the island of inversion starts from ^{31}Mg with the occupation of the [330]1/2 orbit originating from $0f_{7/2}$. We see that the ^{40}Mg nucleus is still largely deformed $\beta_2 = 0.3$. Compared to that in Ne isotopes ($18 < N \leqslant 24$), the deformation region of Mg isotopes is enlarged to $N = 28$ due to the occupation of the "second" intruder orbit with [310]1/2 from $1p_{3/2}$. On the other hand, for Ti, Cr, and Fe isotopes, the magicity of the spherical $0g_{9/2}$ orbit ($N = 50$) is strong and the large deformation is suppressed before the next intruder orbit from $1d_{5/2}$ contributes. This can be attributed to the large level spacing of the first and second intruder orbits at the spherical limit, which respectively comes from $0g_{9/2}$ and $1d_{5/2}$. We expect that the same phenomenon occurs at heavier neutron-rich deformed regions such as the northeast area of ^{132}Sn, in which the next intruder from $1g_{9/2}$ orbit would contribute at $N \approx 110$.

We discuss the effect of the occupation of the second intruder orbits on the density profile. Here, we examine a higher order of the nuclear shape, the hexadecapole deformation parameter, which can be an indicator of the occupation of an elongated orbit [11]. Figure 6 shows the hexadecapole deformation parameters β_4 as a function of the neutron number. As expected, the β_4 value is suddenly enhanced at $N = 60$ due to the occupation of the [550]1/2 orbit, which gives the maximum hexadecapole moment among the orbits with the principal quantum number $n = 5$ [86]. As the neutron number increases, the β_4 value is reduced by the occupation of less elongated orbits. We see a kink behavior at $N \approx 70$. The sizable effect on the β_4 value is found by the occupation of the elongated intruder orbit with [530]1/2 though the degree is smaller than that with [550]1/2. It is desirable to know the isotope dependence of the β_4 values in Zr isotopes experimentally. However, as detailed in Ref. [11], a direct determination of β_4 is not easy by the total reaction cross section measurement based on a simple deformed density model. An elaborated analysis is needed to establish it and this is the next scope of our study.

Additionally, this characteristic behavior of β_2 and β_4 is certainly reflected in the density distribution near the nuclear surface, and its evaluation is meaningful. To quantify the surface density profile, we compute the nuclear diffuseness, which is practically obtained by minimizing the difference between the calculated density distribution and the two-parameter Fermi function with radius (R) and diffuseness (a) parameters. These parameters can be extracted

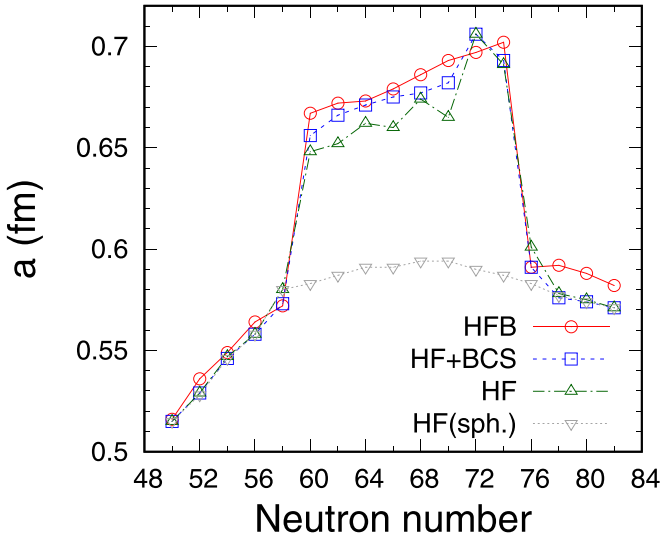

FIG. 7. Nuclear diffuseness of even-even Zr isotopes as a function of neutron number calculated with the HFB, HF+BCS, HF, and spherical-constrained HF models. See text for details.

almost uniquely by measuring the proton-nucleus elastic scattering differential cross section at the first diffraction peak [87]. The thus-obtained a value can be a good measure of the density profile near the nuclear surface and includes a variety of nuclear structure information such as nuclear deformation [9,11], clustering [88,89], bubble structure [90], and core swelling phenomena [54,91,92]. Figure 7 displays the diffuseness parameters of Zr isotopes extracted from the matter density distributions. If the nuclear system exhibits some deformation, the diffuseness value is enhanced in most cases [9–11] due to the occupation of the nodal momentum orbits near the Fermi level [93]. In the spherical region at $50 \leqslant N \leqslant 60$, the a values fall within the range of the standard value about 0.5–0.6 fm [11,86], while it becomes an extremely large value $a \approx 0.7$ fm when the system exhibits large deformation. The behavior at $N \approx 70$–74 is amplified in the a parameters, and therefore the nuclear diffuseness is also sensitive to the occupation of the second intruder orbit and is another possible way to probe the characteristic behavior of nuclear deformation.

Extending these analyses made for Zr isotopes, we also evaluate the quadrupole deformations of neighboring isotopes for a more general understanding of this phenomenon. We find the enlargement of the deformation region in Sr isotopes, which shows similar deformation properties of Zr isotopes. On the other hand, Kr, Mo, and Ru isotopes exhibit some triaxial deformations with less quadrupole deformation compared to the Zr and Sr isotopes. The enlargement of the quadrupole deformation region by the second intruder orbits does not occur in those isotopes.

In summary, we have investigated the nuclear deformation and density profiles of neutron-rich even-even Zr isotopes. The density distributions are generated by the Skyrme-Hartree-Fock-Bogoliubov theory, which can treat both nuclear deformation and paring correlations appropriately. The calculated results are consistent with the quadrupole deformation parameters and point-proton radii deduced from experiments. The anomalously large enhancement of the total reaction cross sections is predicted at $N = 60$ owing to the occupation of the highly elongated intruder orbit originating from the spherical $0h_{11/2}$ orbit. As the neutron number increases, the isotopes keep their large deformation up to $N = 74$. The deformation region is enlarged by the next intruder orbits originating from $1f_{7/2}$ orbits. The signature of the occupation of these intruder orbits can be detected by investigating the nuclear hexadecapole deformation and the density profiles near the nuclear surface. The latter can be observed by using the nucleus-proton elastic scattering. It is highly desirable to systematically measure the total reaction and elastic scattering cross sections for understanding the mechanism of the enlargement of deformation regions and the radius enhancement in heavy mass nuclei $A \gtrsim 110$.

This work was in part supported by JSPS KAKENHI Grants No. 18K03635 and No. 22H01214. We acknowledge the Collaborative Research Program 2022, Information Initiative Center, Hokkaido University.

[1] K. Minomo, T. Sumi, M. Kimura, K. Ogata, Y. R. Shimizu, and M. Yahiro, Phys. Rev. C **84**, 034602 (2011).
[2] M. Takechi, T. Ohtsubo, M. Fukuda, D. Nishimura, T. Kuboki, T. Kubo, T. Suzuki, T. Yamaguchi, A. Ozawa, T. Moriguchi, and H. Ooishi, Phys. Lett. B **707**, 357 (2012).
[3] K. Minomo, T. Sumi, M. Kimura, K. Ogata, Y. R. Shimizu, and M. Yahiro, Phys. Rev. Lett. **108**, 052503 (2012).
[4] T. Sumi, K. Minomo, S. Tagami, M. Kimura, T. Matsumoto, K. Ogata, Y. R. Shimizu, and M. Yahiro, Phys. Rev. C **85**, 064613 (2012).
[5] W. Horiuchi, T. Inakura, T. Nakatsukasa, and Y. Suzuki, Phys. Rev. C **86**, 024614 (2012).
[6] M. Takechi, S. Suzuki, D. Nishimura, M. Fukuda, T. Ohtsubo, M. Nagashima, T. Suzuki, T. Yamaguchi, A. Ozawa, T. Moriguchi *et al.*, Phys. Rev. C **90**, 061305(R) (2014).
[7] S. Watanabe, K. Minomo, M. Shimada, S. Tagami, M. Kimura, M. Takechi, M. Fukuda, D. Nishimura, T. Suzuki, T. Matsumoto *et al.*, Phys. Rev. C **89**, 044610 (2014).
[8] W. Horiuchi, T. Inakura, T. Nakatsukasa, and Y. Suzuki, JPS Conf. Proc. **6**, 030079 (2015).
[9] V. Choudhary, W. Horiuchi, M. Kimura, and R. Chatterjee, Phys. Rev. C **104**, 054313 (2021).
[10] W. Horiuchi and T. Inakura, Prog. Theor. Exp. Phys. **2021**, 103D02 (2021).
[11] W. Horiuchi, T. Inakura, and S. Michimasa, Phys. Rev. C **105**, 014316 (2022).
[12] E. K. Warburton, J. A. Becker, and B. A. Brown, Phys. Rev. C **41**, 1147 (1990).
[13] S. M. Lenzi, F. Nowacki, A. Poves, and K. Sieja, Phys. Rev. C **82**, 054301 (2010).

[14] P. Kienle, T. Faestermann, J. Friese, H.-J. Korner, M. Munch, R. Schneider, A. Stolz, E. Wefers, H. Geissel, G. Munzenberg *et al.*, Prog. Part. Nucl. Phys. **46**, 73 (2001).

[15] T. Sumikama, N. Fukuda, N. Inabe, D. Kameda, T. Kubo, Y. Shimizu, H. Suzuki, H. Takeda, K. Yoshida, H. Baba *et al.*, Phys. Rev. C **103**, 014614 (2021).

[16] J. Erler, N. Birge, M. Kortelainen, W. Nazarewicz, E. Olsen, A. M. Perhac, and M. Stoitsov, Nature (London) **486**, 509 (2012).

[17] M. Yamagami, K. Matsuyanagi, and M. Matsuo, Nucl. Phys. A **693**, 579 (2001).

[18] R. D. O. Llewellyn, M. A. Bentley, R. Wadsworth, H. Iwasaki, J. Dobaczewski, G. deAngelis, J. Ash, D. Bazin, P. C. Bender, B. Cederwall *et al.*, Phys. Rev. Lett. **124**, 152501 (2020).

[19] NuDat 3.0, https://www.nndc.bnl.gov/nudat3/.

[20] F. Browne, A. M. Bruce, T. Sumikama, I. Nishizuka, S. Nishimura, P. Doornenbal, G. Lorusso, P.-A. S'oderstr'om, H. Watanabe, R. Daido *et al.*, Phys. Lett. B **750**, 448 (2015).

[21] N. J. Stone, INDC(NDS)-0833 (2021).

[22] T. Sumikama, K. Yoshinaga, H. Watanabe, S. Nishimura, Y. Miyashita, K. Yamaguchi, K. Sugimoto, J. Chiba, Z. Li, H. Baba *et al.*, Phys. Rev. Lett. **106**, 202501 (2011).

[23] N. Paul, A. Corsi, A. Obertelli, P. Doornenbal, G. Authelet H. Baba, B. Bally, M. Bender, D. Calvet, F. Château *et al.*, Phys. Rev. Lett. **118**, 032501 (2017).

[24] L. Geng, H. Toki, S. Sugimoto, and J. Meng, Prog. Theor. Phys. **110**, 921 (2003).

[25] R. Rodríguez-Guzmán, P. Sarriguren, L. M. Robledo, and S. Perez-Martin, Phys. Lett. B **691**, 202 (2010).

[26] K. Nomura, R. Rodríguez-Guzmán, and L. M. Robledo, Phys. Rev. C **94**, 044314 (2016).

[27] S. Miyahara and H. Nakada, Phys. Rev. C **98**, 064318 (2018).

[28] K. Sieja, F. Nowacki, K. Langanke, and G. Martínez-Pinedo, Phys. Rev. C **79**, 064310 (2009).

[29] T. Togashi, Y. Tsunoda, T. Otsuka, and N. Shimizu, Phys. Rev. Lett. **117**, 172502 (2016).

[30] S. Tagami, Y. R. Shimizu, and J. Dudek, J. Phys. G: Nucl. Part. Phys. **42**, 015106 (2015).

[31] J. Zhao, B. N. Lu, E. G. Zhao, and S. G. Zhou, Phys. Rev. C **95**, 014320 (2017).

[32] B. Kumar, S. K. Singh, and S. K. Patra, Int. J. Mod. Phys. E **24**, 1550017 (2015).

[33] P. Kumar, V. Thakur, S. Thakur, V. Kumar, and S. K. Dhiman, Eur. Phys. J. A **57**, 36 (2021).

[34] J. E. García-Ramos and K. Heyde, Phys. Rev. C **100**, 044315 (2019)

[35] J. E. García-Ramos and K. Heyde, Phys. Rev. C **102**, 054333 (2020).

[36] H. Abusara and S. Ahmad, Phys. Rev. C **96**, 064303 (2017).

[37] W. T. Pinkston and G. R. Satchler, Nucl. Phys. **27**, 270 (1961).

[38] S. Michimasa, Y. Yanagisawa, K. Inafuku, N. Aoi, Z. Elekes, Z. Fülöp, Y. Ichikawa, N. Iwasa, K. Kurita, M. Kurokawa *et al.*, Phys. Rev. C **89**, 054307 (2014).

[39] Y. Yanagisawa, M. Notani, H. Sakurai, M. Kunibu, H. Akiyoshi, N. Aoi, H. Baba, K. Demichi, N. Fukuda, H. Hasegawa *et al.*, Phys. Lett. B **566**, 84 (2003).

[40] N. Aoi, E. Takeshita, H. Suzuki, S. Takeuchi, S. Ota, H. Baba, S. Bishop, T. Fukui, Y. Hashimoto, H. J. Ong *et al.*, Phys. Rev. Lett. **102**, 012502 (2009).

[41] N. Aoi, S. Kanno, S. Takeuchi, H. Suzuki, D. Bazin, M. D. Bowen, C. M. Campbell, J. M. Cook, D.-C. Dinca, A. Gade *et al.*, Phys. Lett. B **692**, 302 (2010).

[42] S. Takeuchi, N. Aoi, T. Motobayashi, S. Ota, E. Takeshita, H. Suzuki, H. Baba, T. Fukui, Y. Hashimoto, K. Ieki *et al.*, Phys. Rev. C **79**, 054319 (2009).

[43] B. Abu-Ibrahim and Y. Suzuki, Phys. Rev. C **61**, 051601(R) (2000).

[44] K. Varga, S. C. Pieper, Y. Suzuki, and R. B. Wiringa, Phys. Rev. C **66**, 034611 (2002).

[45] Y. Suzuki, R. G. Lovas, K. Yabana, and K. Varga, *Structure and Reactions of Light Exotic Nuclei* (Taylor & Francis, London, 2003).

[46] M. Takechi, M. Fukuda, M. Mihara, K. Tanaka, T. Chinda, T. Matsumasa, M. Nishimoto, R. Matsumiya, Y. Nakashima *et al.*, Phys. Rev. C **79**, 061601(R) (2009).

[47] W. Horiuchi, S. Hatakeyama, S. Ebata, and Y. Suzuki, Phys. Rev. C **93**, 044611 (2016).

[48] W. Horiuchi, S. Hatakeyama, S. Ebata, and Y. Suzuki, Phys. Rev. C **96**, 024605 (2017).

[49] T. Nagahisa and W. Horiuchi, Phys. Rev. C **97**, 054614 (2018).

[50] W. Horiuchi and Y. Suzuki, Phys. Rev. C **74**, 034311 (2006).

[51] W. Horiuchi, Y. Suzuki, B. Abu-Ibrahim, and A. Kohama, Phys. Rev. C **75**, 044607 (2007); **76**, 039903(E) (2007).

[52] B. Abu-Ibrahim, S. Iwasaki, W. Horiuchi, A. Kohama, and Y. Suzuki, J. Phys. Soc. Jpn. **78**, 044201 (2009).

[53] W. Horiuchi, Y. Suzuki, P. Capel, and D. Baye, Phys. Rev. C **81**, 024606 (2010).

[54] M. Tanaka, M. Takechi, M. Fukuda, D. Nishimura, T. Suzuki, Y. Tanaka, T. Moriguchi, D. S. Ahn, A. Aimaganbetov, M. Amano *et al.*, Phys. Rev. Lett. **124**, 102501 (2020).

[55] I. Tanihata, H. Hamagaki, O. Hashimoto, Y. Shida, N. Yoshikawa, K. Sugimoto, O. Yamakawa, T. Kobayashi, and N. Takahashi, Phys. Rev. Lett. **55**, 2676 (1985).

[56] M. Fukuda, T. Ichihara, N. Inabe, T. Kubo, H. Kumagai, T. Nakagawa, Y. Yano, I. Tanihata, M. Adachi, K. Asahi, M. Kouguchi, M. Ishihara, H. Sagawa, and S. Shimoura, Phys. Lett. B **268**, 339 (1991).

[57] T. Suzuki, H. Geissel, O. Bochkarev, L. Chulkov, M. Golovkov, D. Hirata, H. Irnich, Z. Janas, H. Keller, T. Kobayashi *et al.*, Phys. Rev. Lett. **75**, 3241 (1995).

[58] M. Fukuda, M. Mihara, T. Fukao, S. Fukuda, M. Ishihara, S. Ito, T. Kobayashi, K. Matsuta, T. Minamisono, S. Momota *et al.*, Nucl. Phys. A **656**, 209 (1999).

[59] T. Suzuki, R. Kanungo, O. Bochkarev, L. Chulkov, D. Cortina, M. Fukuda, H. Geissel, M. Hellström, M. Ivanov, R. Janik *et al.*, Nucl. Phys. A **658**, 313 (1999).

[60] A. Ozawa, T. Kobayashi, T. Suzuki, K. Yoshida, and I. Tanihata, Phys. Rev. Lett. **84**, 5493 (2000).

[61] A. Ozawa, T. Suzuki, and I. Tanihata, Nucl. Phys. A **693**, 32 (2001).

[62] D. Q. Fang, T. Yamaguchi, T. Zheng, A. Ozawa, M. Chiba, R. Kanungo, T. Kato, K. Morimoto, T. Ohnishi, T. Suda, Y. Yamaguchi, A. Yoshida, K. Yoshida, and I. Tanihata, Phys. Rev. C **69**, 034613 (2004).

[63] Y. Yamaguchi, C. Wu, T. Suzuki, A. Ozawa, D. Q. Fang, M. Fukuda, N. Iwasa, T. Izumikawa, H. Jeppesen, R. Kanungo *et al.*, Phys. Rev. C **70**, 054320 (2004).

[64] T. Yamaguchi, T. Suzuki, T. Ohnishi, F. Becker, M. Fukuda, H. Geissel, M. Hosoi, R. Janik, K. Kimura, T. Kuboki *et al.*, Phys. Rev. C **77**, 034315 (2008).

[65] K. Tanaka, T. Yamaguchi, T. Suzuki, T. Ohtsubo, M. Fukuda, D. Nishimura, M. Takechi, K. Ogata, A. Ozawa, T. Izumikawa *et al.*, Phys. Rev. Lett. **104**, 062701 (2010).
[66] K. Tanaka, M. Fukuda, M. Mihara, M. Takechi, D. Nishimura, T. Chinda, T. Sumikama, S. Kudo, K. Matsuta, T. Minamisono *et al.*, Phys. Rev. C **82**, 044309 (2010).
[67] R. Kanungo, A. Prochazka, W. Horiuchi, C. Nociforo, T. Aumann, D. Boutin, D. Cortina-Gil, B. Davids, M. Diakaki, F. Farinon, H. Geissel, R. Gernhäuser, J. Gerl, R. Janik, B. Jonson, B. Kindler, R. Knöbel, R. Krücken, M. Lantz, H. Lenske *et al.*, Phys. Rev. C **83**, 021302(R) (2011).
[68] T. Yamaguchi, K. Tanaka, T. Suzuki, A. Ozawa, T. Ohtsubo, T. Aiba, N. Aoi, H. Baba, M. Fukuda, Y. Hashizume *et al.*, Nucl. Phys. A **864**, 1 (2011).
[69] T. Moriguchi, A. Ozawa, S. Ishimoto, Y. Abe, M. Fukuda, I. Hachiuma, Y. Ishibashi, Y. Ito, T. Kuboki, M. Lantz *et al.*, Phys. Rev. C **88**, 024610 (2013).
[70] T. Moriguchi, A. Ozawa, S. Ishimoto, Y. Abe, M. Fukuda, I. Hachiuma, Y. Ishibashi, Y. Ito, T. Kuboki, M. Lantz *et al.*, Nucl. Phys. A **929**, 83 (2014).
[71] Y. Togano, T. Nakamura, Y. Kondo, J. A. Tostevin, A. T. Saito, J. Gibelin, N. A. Orr, N. L. Achouri, T. Aumann, H. Baba *et al.*, Phys. Lett. B **761**, 412 (2016).
[72] S. Bagchi, R. Kanungo, Y. K. Tanaka, H. Geissel, P. Doornenbal, W. Horiuchi, G. Hagen, T. Suzuki, N. Tsunoda, D. S. Ahn *et al.*, Phys. Rev. Lett. **124**, 222504 (2020).
[73] M. V. Stoitsov, N. Schunck, M. Kortelainen, N. Michel, H. Nam, E. Olsen, J. Sarich, and S. Wild, Comput. Phys. Commun. **184**, 1592 (2013).
[74] J. Bartel, P. Quentin, M. Brack, C. Guet, and H. Håkansson, Nucl. Phys. A **386**, 79 (1982).
[75] N. Sandulescu, P. Schuck, and X. Viñas, Phys. Rev. C **71**, 054303 (2005).
[76] N. Hinohara and W. Nazarewicz, Phys. Rev. Lett. **116**, 152502 (2016).
[77] M. Beiner, H. Flocard, N. V. Giai, and Ph. Quentin, Nucl. Phys. A **238**, 29 (1975).
[78] W. Horiuchi, Y. Suzuki, and T. Inakura, Phys. Rev. C **89**, 011601(R) (2014).
[79] R. J. Glauber, in *Lectures in Theoretical Physics*, edited by W. E. Brittin and L. G. Dunham (Interscience, New York, 1959), Vol. 1, p. 315.
[80] B. Abu-Ibrahim, W. Horiuchi, A. Kohama, and Y. Suzuki, Phys. Rev. C **77**, 034607 (2008); **80**, 029903(E) (2009); **81**, 019901(E) (2010).
[81] P. Campbell, H. L. Thayer, J. Billowes, P. Dendooven, K. T. Flanagan, D. H. Forest, J. A. R. Griffith, J. Huikari, A. Jokinen, R. Moore *et al.*, Phys. Rev. Lett. **89**, 082501 (2002).
[82] I. Angeli and K. P. Marinova, At. Data Nucl. Data Tables **99**, 69 (2013).
[83] Y. Shimizu, T. Kubo, N. Fukuda, N. Inabe, D. Kameda, H. Sato, H. Suzuki, H. Takeda, K. Yoshida, G. Lurusso *et al.*, J. Phys. Soc. Jpn. **87**, 014203 (2018).
[84] T. Ohnishi, T. Kubo, K. Kusaka, A. Yoshida, K. Yoshida, M. Ohtake, N. Fukuda, H. Takeda, D. Kameda, K. Tanaka *et al.*, J. Phys. Soc. Jpn. **79**, 073201 (2010).
[85] S. G. Nilsson, Mat. Fys. Medd. Dan. Vid. Selsk. **29**, 1 (1955).
[86] A. Bohr and B. R. Mottelson, *Nuclear Structure*, Vol. I (W. A. Benjamin, New York, 1975).
[87] S. Hatakeyama, W. Horiuchi, and A. Kohama, Phys. Rev. C **97**, 054607 (2018).
[88] W. Horiuchi and N. Itagaki, Phys. Rev. C **106**, 044330 (2022).
[89] W. Horiuchi and N. Itagaki, Phys. Rev. C **107**, L021304 (2023).
[90] V. Choudhary, W. Horiuchi, M. Kimura, and R. Chatterjee, Phys. Rev. C **102**, 034619 (2020).
[91] W. Horiuchi and T. Inakura, Phys. Rev. C **101**, 061301(R) (2020).
[92] W. Horiuchi and T. Inakura, Phys. Rev. C **105**, 044303 (2022).
[93] W. Horiuchi, Prog. Theor. Exp. Phys. **2021**, 123D01 (2021).